Second order cross-correlation between kinetic Sunyaev-Zel'dovich effect and 21-cm fluctuations from the epoch of reionization

Tashiro, Hiroyuki; Aghanim, Nabila; Langer, Mathieu; Douspis, Marian; Zaroubi, Saleem; Jelic, Vibor

Published in:
Monthly Notices of the Royal Astronomical Society

DOI:
10.1111/j.1365-2966.2011.18644.x

Publication date:
2011

Monthly Notices
of the
ROYAL ASTRONOMICAL SOCIETY

Mon. Not. R. Astron. Soc. **414,** 3424–3433 (2011) doi:10.1111/j.1365-2966.2011.18644.x

Second order cross-correlation between kinetic Sunyaev–Zel'dovich effect and 21-cm fluctuations from the epoch of reionization

Hiroyuki Tashiro,[1,2]★ Nabila Aghanim,[2,3] Mathieu Langer,[2,3] Marian Douspis,[2,3] Saleem Zaroubi[4,5] and Vibor Jelić[6]

[1]*Center for Cosmology, Particle Physics and Phenomenology (CP3), Univ. catholique de Louvain, B-1348 Louvain-la-Neuve, Belgium*
[2]*Univ. Paris-Sud, Institut d'Astrophysique Spatiale, UMR6817, Orsay F-91405, France*
[3]*CNRS, Orsay F-91405, France*
[4]*Kapteyn Astronomical Institute, University of Groningen, PO Box 800, NL-9700AV Groningen, the Netherlands*
[5]*Physics Department, Technion, Haifa 32000, Israel*
[6]*ASTRON, PO Box 2, NL-7990AA Dwingeloo, the Netherlands*

Accepted 2011 March 3. Received 2011 March 3; in original form 2010 August 28

ABSTRACT

The measurement of the brightness temperature fluctuations of neutral hydrogen 21-cm lines from the epoch of reionization (EoR) is expected to be a powerful tool for revealing the reionization process. We study the 21-cm cross-correlation with cosmic microwave background (CMB) temperature anisotropies, focusing on the effect of the patchy reionization. We calculate, up to second order, the angular power spectrum of the cross-correlation between 21-cm fluctuations and the CMB kinetic Sunyaev–Zel'dovich effect (kSZ) from the EoR, using an analytical reionization model. We show that the kSZ and the 21-cm fluctuations are anti-correlated on the scale corresponding to the typical size of an ionized bubble at the observed redshift of the 21-cm fluctuations. The amplitude of the angular power spectrum of the cross-correlation depends on the fluctuations of the ionized fraction. Especially, in a highly inhomogeneous reionization model, the amplitude reaches the order of 100 μK^2 at $\ell \sim 3000$. We also show that second-order terms may help in distinguishing between reionization histories.

Key words: cosmology: theory – large-scale structure of Universe.

1 INTRODUCTION

The epoch of reionization (EoR) is an essential milestone in the formation and evolution of cosmic structure. The first luminous objects produced in collapsed dark matter haloes in the early universe ($z \sim 20$) started to reionize the intergalactic medium (IGM) which was neutral after recombination. Currently we have only a few observations for the EoR. The first one is the Lyα absorption measurement towards high-redshift quasi-stellar objects (QSOs) which probes the fraction of neutral hydrogen along the line of sight (Fan et al. 2006), and the second one is the large-scale cosmic microwave background (CMB) polarization (Komatsu et al. 2011). These observations indicate that the IGM was fully ionized by redshift $z \sim 6$. The recent *HST* observations found large samples of Lyman break galaxies (LBGs) at high redshifts, $7 \lesssim z \lesssim 10$ (Bouwens et al. 2010). Bouwens et al. (2010) have studied reionization with a galaxy model based on these data. Their results suggested that, in addition to such high redshift LBGs, other reionization sources, e.g. faint galaxies and Population III stars, are required to match the optical depth of the *Wilkinson Microwave Anisotropy Probe* (*WMAP*) 7-yr data.

While, current observational data for the EoR are insufficient to study the details of the EoR. In recent years, several observations of signals from the EoR have been suggested to obtain further information about the EoR, for example fluctuations of the neutral hydrogen 21-cm line (Madau, Meiksin & Rees 1997; for a review see Furlanetto, Oh & Briggs 2006), small-scale CMB anisotropies due to the kinetic Sunyaev–Zel'dovich (kSZ; Sunyaev & Zel'dovich 1980; Ostriker & Vishniac 1986; Vishniac 1987, for a review see Aghanim, Majumdar & Silk 2008) and Lyα damping of high-redshift QSOs and gamma-ray bursts (Miralda-Escudé 1998; Barkana & Loeb 2004). While the latter can provide us with information about the end of the EoR, the former two are expected to probe the IGM during the EoR. The

★E-mail: hiroyuki.tashiro@uclouvain.be

Low Frequency Array (LOFAR),[1] Murchison Widefield Array (MWA)[2] and Square Kilometer Array (SKA)[3] are being installed or designed for the measurement of 21-cm line fluctuations, while telescopes such as Atacama Cosmology Telescope (ACT),[4] South Pole Telescope (SPT)[5] and OLIMPO (Masi et al. 2008) will be used to detect and measure the kSZ signal.

Although both autocorrelations of 21-cm lines and CMB anisotropies during the EoR are good probes of the EoR, the cross-correlation between 21-cm fluctuations and the CMB anisotropies created during the EoR is also expected to be useful to study the history of the EoR. The cross-correlation has a potential to provide additional information other than their respective autocorrelations. Besides, the cross-correlation decreases the statistic errors caused by the foreground and the systematic effects, as compared to their autocorrelation. There are several analytical or numerical works about the cross-correlation between CMB and 21-cm fluctuations during the EoR. Alvarez et al. (2006) and Adshead & Furlanetto (2008) computed the expected signal on large scales ($\ell \sim 100$) by analytically calculating the cross-correlation between 21-cm fluctuations and the CMB Doppler anisotropies in the linear regime of the cosmological perturbations. Tashiro et al. (2010) studied the detectability of these signals by LOFAR, MWA and SKA. On small scales ($\ell > 1000$), because the dominant contributions of CMB anisotropies come from the kSZ effect due to the patchiness of the ionized medium, Cooray (2004) has partially studied the cross-correlation with kSZ anisotropies and the second-order 21-cm fluctuations in a simple reionization model. He has also investigated the higher order cross-correlation by calculating the bispectrum. Slosar, Cooray & Silk (2007) have also done the study of the 21-cm cross-correlation with the CMB SZ effect which is caused by hot electrons in the first supernovae remnants during the EoR. Since reionization is a complex physical process, numerical simulations play an important role in the studies of the 21-cm cross-correlation with CMB temperature anisotropies. Numerical works by Jelić et al. (2010) and Salvaterra et al. (2005) focus especially on the small-scale cross-correlation due to the patchy reionization. Additionally, the 21-cm cross-correlation with CMB polarization has been calculated by Tashiro et al. (2008) and Dvorkin, Hu & Smith (2009).

In this paper, we study the cross-correlation between kSZ anisotropies and the second-order 21-cm fluctuations during the EoR analytically. Cooray (2004) has studied this cross-correlation in the simple analytical reionization model where the fluctuations of the ionization fraction are linearly related to the density fluctuations. He concluded that the cross-correlation cannot appear due to the geometric cancellation occurring between the velocity and the density fluctuations. However, the kSZ effect depends strongly on the evolution of the ionization bubbles, and numerical studies of the cross-correlation between 21-cm and kSZ anisotropies also show that patchy reionization generates signals on small scales (Salvaterra et al. 2005). Therefore, we revisit this issue with the analytical model of McQuinn et al. (2005) which produces a reionization history similar to that found in recent numerical simulations.

The outline of our paper is the following. In Section 2, we give the analytical form of the second-order cross-correlation between kSZ anisotropies and 21-cm fluctuations. In Section 3, we give a short description of the analytical reionization model based on McQuinn et al. (2005). In Section 4, we show the angular power spectrum of the second-order cross-correlation, and we discuss the detectability in the case of the SKA sensitivity. Section 5 is devoted to the conclusions. Throughout the paper, we use the concordance cosmological parameters for a flat cosmological model, i.e. $h = 0.73$ ($H_0 = h \times 100\,\mathrm{km\,s^{-1}\,Mpc^{-1}}$), $T_0 = 2.725\,\mathrm{K}$, $\Omega_\mathrm{b} = 0.05$, $\Omega_\mathrm{m} = 0.27$ and $\sigma_8 = 0.9$.

2 THE SECOND-ORDER CROSS-CORRELATION

In this section, we calculate the angular power spectrum of the cross-correlation between 21-cm fluctuations and kSZ anisotropies during the EoR at the second order in the fluctuations. For simplicity, we assume that both fluctuation fields are isotropic statistically. Under this assumption, the angular power spectrum of the cross-correlation C_ℓ is given by

$$\left\langle a^{*\mathrm{kSZ}}_{\ell_1 m_1} a^{21}_{\ell_2 m_2} \right\rangle = \delta^D_{\ell_1 \ell_2} \delta^D_{m_1 m_2} C_{\ell_1}, \tag{1}$$

where $a^{\mathrm{kSZ}}_{\ell_1 m_1}$ and $a^{21}_{\ell_2 m_2}$ are the multipole components of the CMB temperature anisotropies and 21-cm fluctuations during the EoR.

2.1 kSZ CMB anisotropies

During the EoR, secondary CMB temperature anisotropies are caused by the kinetic SZ effect. Their expression is

$$T_{\mathrm{kSZ}}(\hat{\boldsymbol{n}}) = -T_{\mathrm{cmb}} \int^{\eta_0} \mathrm{d}\eta g(\eta) \hat{\boldsymbol{n}} \cdot \boldsymbol{v}(\eta, \hat{\boldsymbol{n}}), \tag{2}$$

where $\boldsymbol{v}$ is the baryon velocity field, $g(\eta)$ is the visibility function at the conformal time η, and the present value of the conformal time is η_0. The visibility function is given by $g(\eta) = \dot{\tau} \mathrm{e}^{-\tau}$, where τ is the optical depth of Thomson scattering from η to today and $\dot{\tau} = \sigma_\mathrm{T} x_\mathrm{i} n_\mathrm{H}$ with σ_T the cross-section of Thomson scattering, x_i the ionized fraction, and n_H the neutral hydrogen density (we ignore the ionization of helium).

We can decompose x_i and n_H into the background and fluctuation values:

$$n_\mathrm{H} = \bar{n}_\mathrm{H}(1 + \delta), \qquad x_\mathrm{i} = \bar{x}_\mathrm{i}(1 + \delta_x), \tag{3}$$

[1] http://www.lofar.org
[2] http://www.mwatelescope.org/
[3] http://www.skatelescope.org
[4] http://www.physics.princeton.edu/act/
[5] http://pole.uchicago.edu/

where the symbols with a bar represent the background values. In equation (3), since we assume that the hydrogen density follows the dark matter density on scales much bigger than the baryonic Jeans length, δ is the total matter density fluctuation field.

Substituting equation (3) into equation (2), we obtain

$$T_{\rm kSZ}(\hat{\boldsymbol{n}}) = -T_{\rm cmb}\int {\rm d}\eta \bar{g}(\eta)\hat{\boldsymbol{n}}\cdot\boldsymbol{v}(\eta,\hat{\boldsymbol{n}})[1+\delta(\eta,\hat{\boldsymbol{n}})+\delta_x(\eta,\hat{\boldsymbol{n}})+\delta(\eta,\hat{\boldsymbol{n}})\delta_x(\eta,\hat{\boldsymbol{n}})]. \tag{4}$$

We focus on the second-order part in equation (4), which can be written in terms of the Fourier components of the fluctuations as

$$\delta T_{\rm kSZ}(\hat{\boldsymbol{n}}) = -{\rm i}T_{\rm cmb}\int {\rm d}\eta \int \frac{{\rm d}^3\boldsymbol{k}}{(2\pi)^3}\int \frac{{\rm d}^3\boldsymbol{k}'}{(2\pi)^3}\bar{g}(\eta)\frac{\hat{\boldsymbol{n}}\cdot(\boldsymbol{k}-\boldsymbol{k}')}{|\boldsymbol{k}-\boldsymbol{k}'|^2}\dot{\delta}(\eta,\boldsymbol{k}-\boldsymbol{k}')[\delta(\eta,\boldsymbol{k}')+\delta_x(\eta,\boldsymbol{k}')]\exp[{\rm i}(\eta_0-\eta)(\hat{\boldsymbol{n}}\cdot\boldsymbol{k})], \tag{5}$$

where we use the relation $\boldsymbol{r} = (\eta_0-\eta)\hat{\boldsymbol{n}}$, and we relate the velocity to δ by the continuity equation in the cosmological linear perturbation theory:

$$\boldsymbol{v} = {\rm i}\frac{\boldsymbol{k}}{k^2}\dot{\delta}(\eta,k), \tag{6}$$

where the dot represents the derivative with respect to η.

Our final aim is to obtain the angular power spectrum of the cross-correlation. Therefore, we consider the spherical harmonic decomposition of equation (5), $a_{\ell m}^{\rm kSZ} = \int {\rm d}\hat{\boldsymbol{n}}\delta T_{\rm kSZ}(\hat{\boldsymbol{n}})Y_\ell^m$. The spherical harmonic coefficients of the kSZ are given by

$$\begin{aligned} a_{\ell m}^{\rm kSZ} = & \sum_{\substack{\ell' m' \ell'' m'' \\ \ell''' m''' m''''}} \int {\rm d}\eta \int \frac{{\rm d}^3\boldsymbol{k}_1}{(2\pi)^3}\int \frac{{\rm d}^3\boldsymbol{k}_2}{(2\pi)^3} \\ & \times A_{\ell\ell'\ell''\ell'''1}^{mm'm''m'''m''''}(\eta)\dot{\delta}(\eta,\boldsymbol{k}_1)[\delta(\eta,\boldsymbol{k}_2)+\delta_x(\eta,\boldsymbol{k}_2)]\frac{j_{\ell'}(k_1 r)}{k_1}j_{\ell''}(k_2 r)Y_{\ell'''}^{m'''}(\hat{\boldsymbol{k}}_1)Y_{\ell''}^{m''}(\hat{\boldsymbol{k}}_2), \end{aligned} \tag{7}$$

where we replaced $\boldsymbol{k}$ and $\boldsymbol{k}'$ by $\boldsymbol{k}_1 \equiv \boldsymbol{k}-\boldsymbol{k}'$ and $\boldsymbol{k}_2 \equiv \boldsymbol{k}'$, and

$$A_{\ell\ell'\ell''\ell'''1}^{mm'm''m'''m''''} = -{\rm i}(-1)^{m+m'-m''+m''''}\frac{64\pi^3}{3}{\rm i}^{\ell'+\ell''}\sqrt{\frac{3(2\ell'+1)}{4\pi(2\ell''''+1)}}C_{-m'-m'''m''''}^{\ell'\ell'''1}C_{000}^{\ell'\ell'''1}M_{\ell\ell'\ell''1}^{-mm'-m''m''''}T_{\rm cmb}\bar{g}(\eta). \tag{8}$$

Here, the $C_{m_1m_2m}^{\ell_1\ell_2\ell}$ are the Clebsch–Gordan coefficients and the $M_{\ell_1\ell_2\ell_3\ell_4}^{m_1m_2m_3m_4}$ are the integrals of quadruple spherical harmonics,

$$\begin{aligned} M_{\ell_1\ell_2\ell_3\ell_4}^{m_1m_2m_3m_4} = & \int {\rm d}\hat{n}Y_{\ell_1}^{m_1}(\hat{n})Y_{\ell_2}^{m_2}(\hat{n})Y_{\ell_3}^{m_3}(\hat{n})Y_{\ell_4}^{m_4}(\hat{n}) \\ = & (-1)^{m_1}\sum_{\ell'm'}\sqrt{\frac{(2\ell_2+1)(2\ell_3+1)(2\ell_4+1)}{16\pi^2(2\ell_1+1)}}C_{m_3m_4m'}^{\ell_3\ell_4\ell'}C_{000}^{\ell_3\ell_4\ell'}C_{m_2m'-m_1}^{\ell_2\ell'\ell_1}C_{000}^{\ell_2\ell'\ell_1}. \end{aligned} \tag{9}$$

2.2 21-cm fluctuations

The brightness temperature of the 21-cm line from a redshift z is given as in Madau et al. (1997) by

$$T_{21}(z) = \frac{\tau_{21}}{(1+z)}(T_{\rm s}-T_{\rm CMB})(z), \tag{10}$$

where $T_{\rm CMB}$ is the CMB temperature and $T_{\rm s}$ is the spin temperature given by the ratio of the number density of hydrogen in the excited state to that of hydrogen in the ground state. The optical depth for the 21-cm line absorption τ_{21} is

$$\tau_{21}(z) = \frac{3c^3\hbar A_{10}x_{\rm H}n_{\rm H}}{16k\nu_{21}^2T_{\rm s}H(z)}, \tag{11}$$

where A_{10} is the Einstein A-coefficient, ν_{21} is the frequency corresponding to the 21-cm wavelength and $x_{\rm H}$ is the fraction of neutral hydrogen, which is written as a function of the ionized fraction $x_{\rm i} = 1-x_{\rm H}$. Note that we drop the redshift space distortion by the peculiar velocity fluctuations of neutral hydrogen in equation (11), although this effect enhances the 21-cm fluctuations (Bharadwaj & Ali 2004).

Combining equation (3) with equations (10) and (11), we can obtain the observed 21-cm fluctuations at the observed frequency ν. The second-order fluctuations which we here focus on is given by

$$\delta T_{21}(\hat{\boldsymbol{n}},\nu) = \int {\rm d}\eta \int \frac{{\rm d}^3\boldsymbol{k}}{(2\pi)^3}\frac{{\rm d}^3\boldsymbol{k}'}{(2\pi)^3}W_{21}[\eta,\eta(z_{\rm obs})]T_0[z(\eta)]\delta(\eta,\boldsymbol{k}-\boldsymbol{k}')\delta_{\rm H}(\eta,\boldsymbol{k}')\exp[{\rm i}(\eta_0-\eta)(\hat{\boldsymbol{n}}\cdot\boldsymbol{k})], \tag{12}$$

where $W_{21}[\eta,\eta(z)]$ is the spectral response function of the observation experiment, normalized as $\int {\rm d}\eta W_{21}[\eta,\eta(z)] = 1$ and centred at $\eta(z)$, the redshift $z_{\rm obs}$ is related to the frequency ν as $\nu = \nu_{21}/(1+z_{\rm obs})$, $\delta_{\rm H} \equiv (x_{\rm H}-\bar{x}_{\rm H})/\bar{x}_{\rm H}$ and T_0 is a normalization temperature factor given by

$$T_0(z) = 23\left(\frac{\Omega_{\rm b}h^2}{0.02}\right)\left[\left(\frac{0.15}{\Omega_{\rm m}h^2}\right)\left(\frac{1+z}{10}\right)\right]^{1/2}\left(\frac{T_{\rm s}-T_{\rm cmb}}{T_{\rm s}}\right){\rm mK}. \tag{13}$$

The spin temperature is determined by three couplings with CMB, IGM gas and Lyα photons. In the EoR, Lyα photons emitted from ionizing sources couple the spin temperature with the IGM gas temperature (Ciardi & Madau 2003). Meanwhile, since the IGM gas is heated up quickly by Lyα and X-ray photons from stars and QSOs, the IGM gas temperature is much higher than the CMB temperature during reionization. Therefore, we can assume $T_{\rm s} \gg T_{\rm cmb}$ during the EoR in equation (13).

Taking the harmonic decomposition, we obtain the spherical harmonic coefficients of the 21-cm fluctuations:

$$a_{\ell m}^{21} = \sum_{\ell' m'} \sum_{\ell'' m''} \int \mathrm{d}\eta \int \frac{\mathrm{d}^3 \boldsymbol{k_1}}{(2\pi)^3} \int \frac{\mathrm{d}^3 \boldsymbol{k_2}}{(2\pi)^3} B^{mm'm''}(\eta) \delta(\eta, \boldsymbol{k}_1) \delta_{\mathrm{H}}(\eta, \boldsymbol{k}_2) j_{\ell'}(k_1 r) j_{\ell''}(k_2 r) Y_{\ell'}^{m'*}(\hat{\boldsymbol{k}}_1) Y_{\ell''}^{m''*}(\hat{\boldsymbol{k}}_2), \tag{14}$$

where

$$B^{mm'm''}(\eta) = 16\pi^2 i^{\ell'+\ell''} W_{21}(\eta) T_0(\eta) M_{\ell'\ell''\ell}^{m'm''-m}. \tag{15}$$

Here $M_{\ell_1\ell_2\ell_3}^{m_1m_2m_3}$ is the integral of triple spherical harmonics:

$$\begin{aligned} M_{\ell_1\ell_2\ell_3}^{m_1m_2m_3} &= \int \mathrm{d}\hat{n} Y_{\ell_1}^{m_1}(\hat{n}) Y_{\ell_2}^{m_2}(\hat{n}) Y_{\ell_3}^{m_3}(\hat{n}) \\ &= (-1)^{m_1} \sqrt{\frac{(2\ell_2+1)(2\ell_3+1)}{4\pi(2\ell_1+1)}} C_{m_2 m_3 - m_1}^{\ell_2\ell_3\ell_1} C_{000}^{\ell_2\ell_3\ell_1}, \end{aligned} \tag{16}$$

where $m_1 + m_2 = m_3$.

2.3 The cross-correlation

The second-order cross-correlation is given by substituting equations (7) and (14) into equation (1). We obtain

$$\begin{aligned} C_\ell^{\mathrm{kSZ-21}} = &- \sum_{\ell_1' m_1'} \sum_{\ell_1'' m_1''} \sum_{\substack{\ell_2' m_2' \\ \ell_2'' m_2'' m_2''' \\ \ell_2''' m_2'''}} \int \mathrm{d}\eta \int \mathrm{d}\eta' \int \frac{\mathrm{d}^3 \boldsymbol{k_1}}{(2\pi)^3} \int \frac{\mathrm{d}^3 \boldsymbol{k_2}}{(2\pi)^3} \int \frac{\mathrm{d}^3 \boldsymbol{k_1'}}{(2\pi)^3} \int \frac{\mathrm{d}^3 \boldsymbol{k_2'}}{(2\pi)^3} \\ & \left\langle \delta^*(\eta, \boldsymbol{k}_1) \delta_x^*(\eta, \boldsymbol{k}_2) \dot{\delta}(\eta', \boldsymbol{k}_1') [\delta(\eta', \boldsymbol{k}_2') + \delta_x(\eta', \boldsymbol{k}_2')] \right\rangle A_{\ell\ell_2'\ell_2'' 1 \ell_2'''}^{mm_2'm_2''m_2'''m_2''''}(\eta') [B^{m-m_1'-m_1''}(\eta)]^* \\ & \times j_{\ell_1'}(k_1 r) j_{\ell_1''}(k_2 r) \frac{j_{\ell_2'}(k_1' r')}{k_1'} j_{\ell_2''}(k_2' r') Y_{\ell_1'}^{m_1'*}(\hat{\boldsymbol{k}}_1) Y_{\ell_1''}^{m_1''*}(\hat{\boldsymbol{k}}_2) Y_{\ell_2''''}^{m_2''''}(\hat{\boldsymbol{k}}_1') Y_{\ell_2''}^{m_2''}(\hat{\boldsymbol{k}}_2'), \end{aligned} \tag{17}$$

where $r' = \eta_0 - \eta'$ and we use $\delta_x = -\delta_{\mathrm{H}}$.

Under the assumption that all fluctuation fields are Gaussian, the Wick theorem breaks the ensemble average in equation (17) into components with $\langle\delta\delta\rangle$, $\langle\delta_x\delta_x\rangle$ and $\langle\delta\delta_x\rangle$. For the simplification of equation (17), we assume that $W_{21}(z) = \delta(z - z_{\mathrm{obs}})$. This is a good approximation because, compared to the observed frequency, the spectral resolution is narrow (for example, the spectral resolution in the LOFAR case is less than 1 MHz while the observed frequency is about 150 MHz for $z_{\mathrm{obs}} \sim 10$.). We can simplify further by using the approximation for the integration of spherical Bessel functions with $\ell \gg 1$,

$$\int \mathrm{d}r' \int \mathrm{d}k k^2 F(k) j_\ell(kr) j_\ell(kr') \approx \int \mathrm{d}r' \frac{\pi}{2} \frac{\delta(r - r')}{r^2} F(k) \Big|_{k=\ell/r} = \frac{\pi}{2} \frac{F(\ell/r)}{r^2}. \tag{18}$$

Finally, we can rewrite the cross-correlation as

$$\begin{aligned} C_\ell^{\mathrm{kSZ-21}} = &- \sum_{\ell_1\ell_2} \frac{(2\ell_2+1)(2\ell_1+1)}{2\pi^2(2\ell+1)} \left| C_{000}^{\ell_1\ell_2\ell} \right|^2 \frac{T_0(\eta_{\mathrm{obs}}) T_{\mathrm{cmb}}}{H_{\mathrm{obs}} r_{\mathrm{obs}}^2} \frac{\dot{G}(\eta_{\mathrm{obs}})}{G(\eta_{\mathrm{obs}})} \bar{g}(\eta_{\mathrm{obs}}) \int \mathrm{d}k j_{\ell_1}(kr_{\mathrm{obs}}) \frac{\mathrm{d}j_{\ell_1}(kr)}{\mathrm{d}r} \Big|_{r=r_{\mathrm{obs}}} \\ & \times \left[\left(P_{\delta x}\left(\eta_{\mathrm{obs}}, \frac{\ell_2}{r}\right) + P_{xx}\left(\eta_{\mathrm{obs}}, \frac{\ell_2}{r}\right) \right) P_{\delta\delta}(\eta_{\mathrm{obs}}, k) + \left(P_{\delta\delta}\left(\eta_{\mathrm{obs}}, \frac{\ell_2}{r}\right) + P_{\delta x}\left(\eta, \frac{\ell_2}{r}\right) \right) P_{\delta x}(\eta_{\mathrm{obs}}, k) \right] \Big|_{r=r_{\mathrm{obs}}}, \end{aligned} \tag{19}$$

where the power spectra $P_{\delta\delta}$, P_{xx} and $P_{\delta x}$ are defined as $\langle\delta(\eta, k_1)\delta(\eta, k_2)\rangle = (2\pi)^3\delta(k_1 - k_2)P_{\delta\delta}(\eta, k_1)$, $\langle\delta_x(\eta, k_1)\delta_x(\eta, k_2)\rangle = (2\pi)^3\delta(k_1 - k_2)P_{xx}(\eta, k_1)$, and $\langle\delta(\eta, k_1)\delta_x(\eta, k_2)\rangle = (2\pi)^3\delta(k_1 - k_2)P_{\delta x}(\eta, k_1)$. In equation (19), G is the growth factor of the dark matter density fluctuations which is $\delta(k, \eta) = G(\eta)\delta(k)$ with the present density fluctuations $\delta(k)$. Now, the epoch we are interested in is matter dominated, so that we can assume $G \propto 1/(1 + z)$ in terms of the redshift z.

In order to calculate the cross-correlation, the power spectra P_{xx} and $P_{\delta x}$ which are determined by the reionization model are essential. We discuss the analytical reionization model in the following section.

3 REIONIZATION MODEL

For an analytical reionization model, we adopt the approach of Furlanetto, Zaldarriaga & Hernquist (2004b) and McQuinn et al. (2005). Ionization bubbles start to evolve from high-density galaxy regions into the voids, as shown in recent numerical simulations (e.g. Trac & Gnedin 2009, and references therein). Therefore, the mass of ionized gas m_{ion} is associated with the mass of a collapsed object m_{gal} by the ansatz, $m_{\mathrm{ion}} = \zeta m_{\mathrm{gal}}$ where ζ is an ionizing efficiency. The condition for the full ionization of a region of mass m is that the region contains sufficient sources to self-ionize, i.e. $f_{\mathrm{coll}} \geq \zeta^{-1}$, where f_{coll} is the fraction of collapsed haloes above the critical mass for collapse, m_{min} (Lacey & Cole 1993).

This criterion gives the barrier (the density threshold) δ_x for 'self-ionization' which depends on m. Furlanetto, Zaldarriaga & Hernquist (2004a) found a reasonable approximation of the barrier in the linear form of the variance of the density fluctuations, $\sigma^2(m, z)$, as

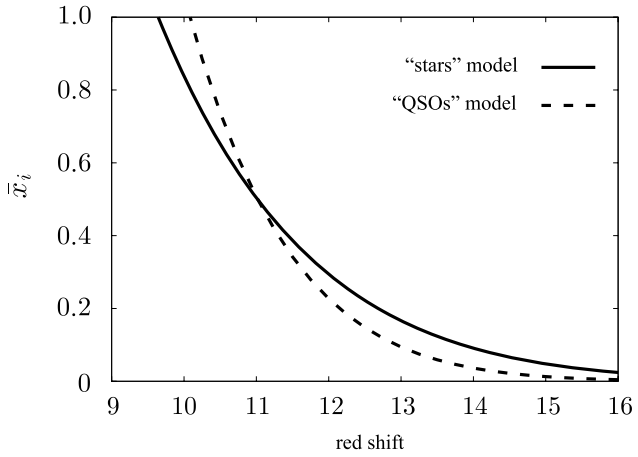

Figure 1. Evolution of the mean ionized fraction. The solid and dotted lines represent $\bar{x}_{\rm i}$ in the 'stars' and 'QSOs' models, respectively.

$B(m, z) = B_0 + B_1\sigma^2(m, z)$, where $\sigma(m, z)$ is obtained by smoothing the density field at the scale m. Here, $B_0 = \delta_{\rm c} - \sqrt{2}K(\zeta)\sigma_{\rm min}(z)$ and $B_1 = \partial\delta_x/\partial\sigma^2|_{\sigma^2=0}$, where $\sigma_{\rm min}(z)$ is the mass dispersion at the minimum mass and redshift z for the collapsed ionization source.

For the linear barrier $B(m, z)$, the bubble mass function is written as (Sheth 1998)

$$\frac{{\rm d}n(m)}{{\rm d}m}{\rm d}m = \sqrt{\frac{2}{\pi}}\frac{\bar{\rho}}{m^2}\left|\frac{{\rm d}\log\sigma}{{\rm d}\log m}\right|\frac{B_0}{\sigma(m)}\exp\left[-\frac{B^2(m,z)}{2\sigma^2(m)}\right]{\rm d}m\,, \tag{20}$$

where $\bar{\rho}$ is the mean mass density of the Universe.

The smallest bubble mass is given by $\zeta m_{\rm min}$. Therefore, we can obtain the mean ionized fraction (volume averaged) $\bar{x}_{\rm i}$ as

$$\bar{x}_{\rm i} = \int_{\zeta m_{\rm min}} V(m)\frac{{\rm d}n(m)}{{\rm d}m}{\rm d}m = \frac{1}{2}{\rm e}^{-2B_0B_1}{\rm erfc}\left(\frac{B_0 - B_1\sigma_\zeta^2}{\sqrt{2\sigma_\zeta^2}}\right) + \frac{1}{2}{\rm erfc}\left(\frac{B_0 + B_1\sigma_\zeta^2}{\sqrt{2\sigma_\zeta^2}}\right), \tag{21}$$

where $\sigma_\zeta = \sigma(\zeta m, z)$ and $V(m)$ is the comoving volume of a bubble with mass m.

In the case of a linear barrier, the linear bias of a source of mass m is given by (McQuinn et al. 2005)

$$b(m) = 1 + \frac{B(m)/\sigma^2(m) - 1/B_0}{D(z)}. \tag{22}$$

Therefore, the mean bias of the bubble $\bar{b}(m)$ is obtained from

$$\bar{b} = \bar{x}_{\rm i}^{-1}\int {\rm d}m\, b(m)V(m)\frac{{\rm d}n(m)}{{\rm d}m}. \tag{23}$$

In this reionization model, the free parameters for the model are ζ and $m_{\rm min}$. Here we take two parameter sets which are motivated from numerical simulations: 'stars' model and 'QSOs' model (Jelić et al. 2010). In both models, the ionized fraction reaches $\bar{x}_{\rm i} = 0.5$ at $z = 11$, in order to agree with the *WMAP* results.

In the 'stars' model, we assume that stars are responsible for reionization. We take a low efficiency $\zeta \approx 40$ which is reasonable for normal star formation and assume that the minimum mass corresponds to a virial temperature of 10^4 K, above which cooling by atomic hydrogen becomes efficient.

In the 'QSOs' model, we assume that the reionization history is faster and the bubble size is larger compared to those in the 'stars' model. Therefore, we set high a virial temperature (5×10^4 K) and a high efficiency $\zeta \approx 200$. The candidates for the ionization sources are massive stars and QSOs.

We show the evolution of the ionized fraction for each model in Fig. 1. From equation (20), we can obtain the bubble size distribution $V{\rm d}n/{\rm d}R$ as a function of the comoving size R of a bubble under the assumption that the bubbles are spherical. We plot the results in Fig. 2.

3.1 The two-point correlation function $\xi_{xx}(r)$

In order to obtain the power spectra P_{xx} and $P_{\delta x}$ in equation (19), we need to compute the correlation function $\xi_{xx}(r) = \langle x_{\rm i}(\boldsymbol{x}_1)x_{\rm i}(\boldsymbol{x}_2)\rangle - \bar{x}_{\rm i}^2$ and $\xi_{\delta x}(r) = \langle\delta(\boldsymbol{x}_1)x_{\rm i}(\boldsymbol{x}_2)\rangle$, where the points $\boldsymbol{x}_1$ and $\boldsymbol{x}_2$ are separated by $r = |\boldsymbol{x}_1 - \boldsymbol{x}_2|$. Here we utilize the analytical correlation functions of McQuinn et al. (2005).

As in the case of the density correlation function in the halo formalism, the correlation function of the ionized fraction $\xi_{xx}(r)$ receives two contributions. One is a one bubble term P_1 which is the two-point correlation for the case where two points which are separated by r are ionized by the one and same ionization source, the other is a two bubble term P_2 which corresponds to the case where two points are ionized by two separate sources. As shown in Fig. 2, the typical size of an ionization bubble becomes larger than 5 Mpc when the ionized fraction reaches one half. In such regime, where the ionization bubbles become large, P_1 is largely dominant and P_2 can be ignored. Thus,

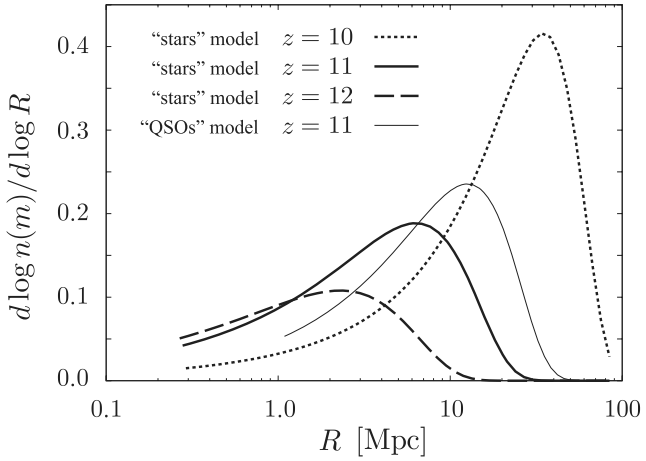

Figure 2. Ionized bubble comoving size distribution. The dotted, solid and dashed lines represent the distributions in the 'stars' model at $z = 10$, 11 and 12, respectively. The ionized fractions are $\bar{x}_{\rm i} = 0.8$ at $z = 10$, $\bar{x}_{\rm i} = 0.5$ at $z = 11$ and $\bar{x}_{\rm i} = 0.3$ at $z = 12$. We also plot the distribution in the 'QSOs' model at $z = 11$ as the thin solid line. The left side of each line ends at $R(\zeta m_{\rm min})$ where $\zeta m_{\rm min}$ is the minimum mass of the ionized region.

McQuinn et al. (2005) divide the reionization process into two phases: the early phase and the late phase. In the early phase, both P_1 and P_2 are important, while in the late phase, P_1 is dominant and P_2 can be ignored. The criterion for these phases is set as $\bar{x}_{\rm i} > 0.5$ in order to be in agreement with results from the hybrid approach of analytic modelling and numerical simulations of Zahn et al. (2005). They define the correlation function $\xi_{xx}(r)$ by

$$\xi_{xx}(r) = \begin{cases} (1 - \bar{x}_{\rm i})\, P_1(r) & \text{when } \bar{x}_{\rm i} > 0.5, \\ P_1(r) + P_2(r) - \bar{x}_{\rm i}^2 & \text{otherwise,} \end{cases} \tag{24}$$

where

$$P_1(r) = \int {\rm d}m\, \frac{{\rm d}n(m)}{{\rm d}m} V_0(m, r), \tag{25}$$

$$P_2(r) = \int {\rm d}m_1 \frac{{\rm d}n(m_1)}{{\rm d}m} \int {\rm d}^3\boldsymbol{r}_1 \int {\rm d}m_2 \frac{{\rm d}n(m_2)}{{\rm d}m} \int {\rm d}^3\boldsymbol{r}_2 [1 + \xi(\boldsymbol{r}_1 - \boldsymbol{r}_2 | m_1, m_2)]. \tag{26}$$

Here, $\xi(r|m_1, m_2)$ is the excess probability to have a bubble of mass m_1 at the distance r from a bubble of mass m_2. For the simplicity of the calculation, it is assumed that $\xi(r|m_1, m_2)$ can be written in terms of the correlation function of the matter density $\xi_{\delta\delta}$ as $\xi(r|m_1, m_2) = \bar{b}\xi_{\delta\delta}[\max(r, R_1 + R_2)]$, where $R_1(m_1)$ and $R_2(m_2)$ are the bubble radii.

In order to calculate the volume in equations (25) and (26) analytically, all ionization bubbles are assumed spherical. Therefore, $V_0(m, r)$ is the volume within a sphere of mass m that can encompass two points separated by a distance r. For the volume integration in equation (26), McQuinn et al. (2005) adopt the overlapping conditions: (1) m_1 cannot ionize r_2, and m_2 cannot ionize r_1; (2) the centre of m_2 cannot lie inside m_1, but any other part of m_2 *can* touch m_1, and vice versa.

3.2 The two-point cross-correlation function $\xi_{\delta x}(r)$

As in the case of $\xi_{xx}(r)$, the two-point cross-correlation $\xi_{\delta x}(r)$ has two contributions, $P_{\rm in}$ and $P_{\rm out}$. The contribution $P_{\rm in}$ corresponds to the case of both points being contained within the same ionized bubble. Following McQuinn et al. (2005), it is written as

$$\begin{aligned} P_{\rm in}(r) &= \int {\rm d}m \frac{{\rm d}n(m)}{{\rm d}m} V_0(m, r) \int {\rm d}m_{\rm h} \frac{m_{\rm h}}{\rho} \frac{{\rm d}n_{\rm h}(m_{\rm h}|m)}{{\rm d}m_{\rm h}} \\ &= \int {\rm d}m \frac{{\rm d}n(m)}{{\rm d}m} V_0(m, r)[1 + B(m, z)], \end{aligned} \tag{27}$$

where the last line in equation (27) is obtained by using the fact that the inner integral is the mean overdensity of the bubble $1 + \delta_B$ and δ_B is $B(m, z)$ at linear order.

The contribution $P_{\rm out}$ corresponds to the case when one point is outside the ionized bubble of the other point. McQuinn et al. (2005) give $P_{\rm out}$ in terms of the mean bias for haloes $\bar{b}_{\rm h}$,

$$P_{\rm out}(r) = \bar{x}_{\rm i} - \int {\rm d}m \frac{{\rm d}n(m)}{{\rm d}m} V_0(m, r) + \int {\rm d}m \frac{{\rm d}n(m)}{{\rm d}m} \int {\rm d}^3\boldsymbol{r}_{\rm b} [\bar{b}_{\rm h}\bar{b}\xi_{\delta\delta}(\boldsymbol{r} - \boldsymbol{r}_{\rm b})]. \tag{28}$$

where ${\rm d}n_{\rm h}(m_{\rm h}|m)/{\rm d}m_{\rm h}$ is the conditional mass function. In equation (28), the integration range of $\boldsymbol{r}_{\rm b}$ is over all bubbles which ionize the point $\boldsymbol{r}_{\rm b}$ but not the other point separated by $\boldsymbol{r}$ from $\boldsymbol{r}_{\rm b}$. For simplicity, $\xi_{\delta\delta}$ is evaluated at the separation $\max[R(m), r]$.

As the reionization proceeds and the typical size of an ionized bubble becomes large, the term $P_{\rm out}$ becomes unimportant as compared to $P_{\rm in}$. Therefore, the computation of $\xi_{\delta x}$ is divided into two phases again:

$$\xi_{\delta x}(r) = \begin{cases} P_{\rm in} - P_{\rm l} & \text{when } \bar{x}_{\rm i} > 0.5, \\ P_{\rm in} + P_{\rm out} - \bar{x}_{\rm i} & \text{otherwise,} \end{cases} \tag{29}$$

where we assume that $P_{\rm in}$ is dominant in large $\bar{x}_{\rm i}$ ($\bar{x}_{\rm i} > 0.5$), and we subtract $P_{\rm l}$ given by equation (27) from $P_{\rm in}$ which is the correlation between $x_{\rm i}$ and $\rho/\bar{\rho}$.

4 RESULTS AND DISCUSSION

We calculate the angular power spectrum of the cross-correlation described in equation (19) in the two models, 'stars' and 'QSOs'. First, we show the results in the 'stars' model in Fig. 3. In this model, the mean ionized fraction is 0.3, 0.5 and 0.8 at $z = 12$, 11 and 10, respectively. The signal of the cross-correlation between kSZ and 21-cm fluctuations exhibits an anti-correlation on small scales ($\ell > 1000$). As mentioned in Cooray (2004), there is a geometric cancellation in the cross-correlation. This cancellation is responsible for a suppression of the amplitude of the cross-correlation. However, the cross-correlation has a distinctive oscillatory shape. Especially, we found that the peak position of the anti-correlation represents the typical size of an ionized bubble at each redshift. For example, at $z = 11$, the typical size of an ionized bubble is almost 6 Mpc, as shown in Fig. 2, and the anti-correlation at $z_{\rm obs} = 11$ is maximal at the corresponding multipole $\ell \sim 4000$. As the Universe

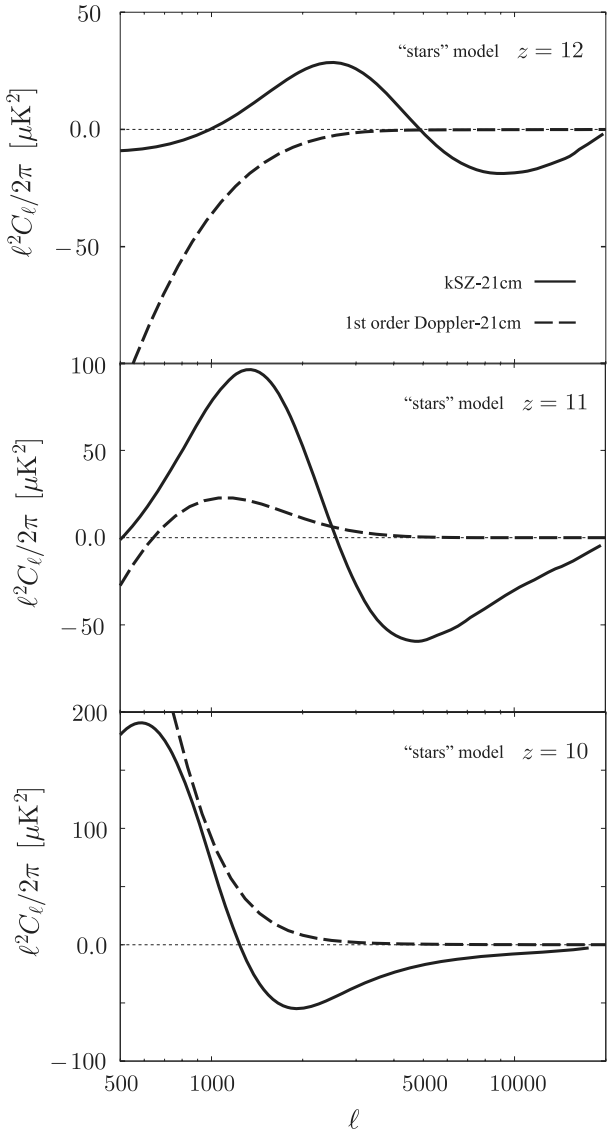

Figure 3. Angular power spectra of the second-order cross-correlation in the 'stars' model. From top to bottom panels, we plot the angular power spectra at $z_{\rm obs} = 12$, 11 and 10, respectively. The mean ionized fraction is $\bar{x} = 0.8$ at $z = 10$, $\bar{x} = 0.5$ at $z = 11$ and $\bar{x} = 0.3$ at $z = 12$. For reference, we show the first-order cross-correlation between the CMB temperature and 21-cm fluctuations as the dotted line in each panel.

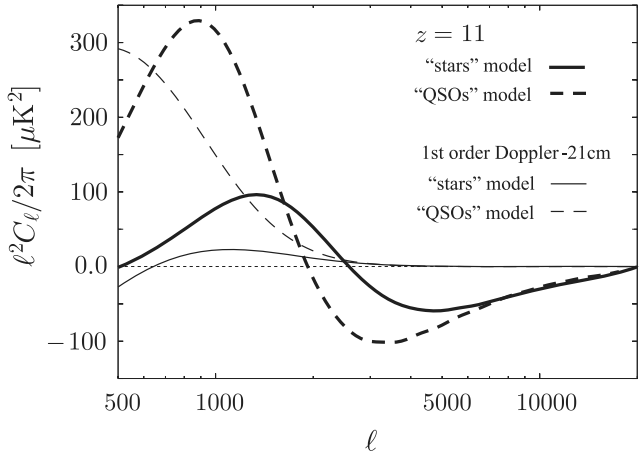

Figure 4. Dependence of the cross-correlation on the ionization model. The solid and the dashed lines are the power spectrum for the 'stars' model and the 'QSOs' model, respectively (see text). We set $z_{\rm obs} = 11$ where $\bar{x} = 0.5$ in both models. For reference, we plot the first-order cross-correlation in each model as the thin lines.

evolves, the typical scale of an ionized bubble becomes larger. The peak position of the anti-correlation shifts accordingly towards smaller values.

The evolution of the cross-correlation amplitude depends on the evolution of δ_x through the power spectra of P_{xx} and $P_{x\delta}$ which evolve rapidly during the EoR. Since the amplitudes of P_{xx} and $P_{x\delta}$ increase as the redshift decreases, the amplitude of the cross-correlation also becomes larger at low redshifts. However, after the average ionization rate reaches $\bar{x}_{\rm i} \sim 0.9$, the signal of the 21-cm fluctuations becomes weak and the cross-correlation amplitude also starts to decrease.

In Fig. 3, we also plot the first-order cross-correlation between 21-cm and CMB Doppler anisotropies calculated by using the same expression as equation (15) of Alvarez et al. (2006). The sign of the first-order cross-correlation depends on the evolution of δ_x. As long as δ_x is small, the ionization process is homogeneous, and the cross-correlation is negative. On the other hand, in the case of a highly inhomogeneous reionization, the sign of the cross-correlation is positive. In our reionization model, the first-order cross-correlation at the early phase of reionization is negative at $\ell < 1000$ (see the top and middle panels in Fig. 3). We found the amplitude of the first-order cross-correlation at $z_{\rm obs} = 11$ is $300\,\mu{\rm K}^2$ at the peak position, $\ell \sim 100$, and decreases rapidly towards zero at large multipoles. As we can see in Fig. 3, the second-order kSZ–21 cm cross-correlation dominates the first-order cross-correlation at multipoles larger than $\ell = 1000$. However, as the ionization process proceeds, the ionization fraction is highly inhomogeneous and δ_x is evolved well. As a result, the first-order cross-correlation has a positive sign and a high amplitude as shown in the bottom panel of Fig. 3. The first-order cross-correlation becomes comparable to the second-order kSZ–21 cm cross-correlation even at $\ell \sim 1000$, while the kSZ cross-correlation still dominates the first-order cross-correlation and has negative correlation at multipoles higher than $\ell = 1000$.

Next we show the dependence of the angular cross-correlation power spectrum on the ionization model in Fig. 4. In the 'QSOs' model, the ionization history is rapid and the typical size of ionized bubbles is large. The amplitude of P_{xx} and $P_{x\delta}$ in the 'QSOs' model is larger than in the 'stars' model. As a result, in the 'QSOs' model, the signal of the cross-correlation is large and the peak position of the anti-correlation appears on small multipoles, as expected. We can therefore conclude that the cross-correlation between kSZ and 21-cm fluctuations at the second order is sensitive to the average size of an ionized bubble. The first-order cross-correlation also has a higher amplitude than in the 'stars' model because the amplitude depends on the evolution rate of the background ionization fraction. However, the inhomogeneous contribution coming from the term with $P_{x\delta}$ in equation (15) in Alvarez et al. (2006) is partially cancelled by the homogeneous one from the term with $P_{\delta\delta}$. As a result, in the highly inhomogeneous 'QSOs' reionization model, the cross-correlation between kSZ and second-order 21-cm fluctuations reaches a significant amplitude, compared with the first-order cross-correlation at small scales ($\ell \lesssim 1000$).

4.1 Detectability

In the previous section, we showed that the peak position of the anti-correlation is related to the typical bubble size at the observed redshift of 21-cm fluctuations. Here, our concern is the detectability of such negative peak in the kSZ–21 cm cross-correlation. In order to investigate the detectability, we calculate the signal-to-noise ratio (S/N). For simplicity, we assume that CMB, 21-cm fluctuations and instrumental noise are Gaussian. The total S/N can be calculated as

$$\left(\frac{\rm S}{\rm N}\right)^2 = f_{\rm sky} \sum_{\ell=\ell_{\rm min}}^{\ell_{\rm max}} (2\ell+1) \frac{\left|C_\ell^{21-{\rm CMB}}\right|^2}{\left|C_\ell^{21-{\rm CMB}}\right|^2 + C_\ell^{21} C_\ell^{\rm CMB}}, \tag{30}$$

where $f_{\rm sky}$ is the sky fraction common to the two cross-correlated signals, and $C_\ell^{\rm CMB}$, C_ℓ^{21} and $C_\ell^{21-{\rm CMB}}$ are the angular power spectra of CMB, 21-cm fluctuation and the cross-correlation between 21-cm and CMB, respectively. In order to focus on the detectability of the signal from the typical bubble size, we set $\ell_{\rm min} = 500$ and $\ell_{\rm max} = 5000$.

At the multipoles that we are interested in ($\ell > 1000$), the dominant CMB signal is due to the thermal SZ effect (Zel'dovich & Sunyaev 1969). However, we can remove this contribution because of the frequency dependence of the SZ effect. Therefore, with the assumption that the foreground can be completely removed from the CMB map, the main contribution to $C_l^{\rm CMB}$ comes from the primordial CMB anisotropies $C_\ell^{\rm pri}$ and the noise of the instrument $N_\ell^{\rm CMB}$. We can write $C_\ell^{\rm CMB}$ as

$$C_\ell^{\rm CMB} = C_\ell^{\rm pri} \exp\left(-\ell^2 \sigma_{\rm CMB}^2/2\right) + N_\ell^{\rm CMB}, \tag{31}$$

where we assume the beam profile of CMB observation is Gaussian with the full width at half-maximum (FWHM) of the beam $\theta_{\rm CMB}$, and $\sigma_{\rm CMB} = \theta_{\rm CMB}/\sqrt{8\ln 2}$. The effect of the beam size is a damping of the signal of the primordial CMB on smaller scales than the FWHM. The noise power spectrum $N_\ell^{\rm CMB}$ is given by (Knox 1995)

$$N_\ell^{\rm CMB} = \sigma_{\rm pix}^2 \Omega_{\rm pix}, \tag{32}$$

where $\sigma_{\rm pix}$ is the sensitivity in each pixel and $\Omega_{\rm pix}$ is the solid angle per pixel; $\Omega_{\rm pix} = \theta_{\rm CMB}^2$.

As for the 21-cm fluctuations, the noise signal from the instruments and foreground will dominate the intrinsic signal from the EoR. Assuming that the foreground can be removed to the level below the noise from instruments, we can write

$$C_\ell^{21} = N_\ell^{21} = \frac{2\pi}{t_{\rm obs}\Delta\nu}\left(\frac{D\lambda}{A/T}\right)^2, \tag{33}$$

where we use the noise power spectrum of 21-cm observation estimated by Zaldarriaga, Furlanetto & Hernquist (2004). In equation (33), $\Delta\nu$ is the bandwidth, $t_{\rm obs}$ is the total integration time, A/T is the sensitivity (an effective area divided by the system temperature) and D is the length of the baseline associated with the FWHM of the 21-cm observation $\theta_{21} = \lambda/D$.

In the calculation of the cross-correlation signal, we assume that the foregrounds and noise of 21-cm fluctuations and CMB anisotropy are not correlated. Therefore, the cross-correlation consists mainly of the first-order Doppler 21-cm cross-correlation and the second-order kSZ–21 cm one,

$$\left|C_\ell^{21-{\rm CMB}}\right|^2 = \left(\left|C_\ell^{21-{\rm Dopper}}\right|^2 + \left|C_\ell^{21-{\rm kSZ}}\right|^2\right) \exp[-\ell^2\left(\sigma_{\rm CMB}^2 + \sigma_{21}^2\right)/2], \tag{34}$$

where $\sigma_{21} = \theta_{21}/\sqrt{8\ln 2}$ and both signals are affected by the angular resolution of the observations.

Our interest is the detectability of the cross-correlation signal from the patchy reionization by *Planck* and SKA. Therefore, in the computation of equation (31), we adopt the typical value of *Planck* which are $\theta_{\rm CMB} = 5$ arcmin and $\sigma_{\rm pix} = 5 \times 10^{-6}$. The goal sensitivity of SKA is currently designed as $A/T = 5000\,{\rm m^2\,K^{-1}}$ at 200 MHz. The configuration area is 20 per cent of total collecting area for 1-km baseline, 50 per cent for 5-km baseline, 75 per cent for 150-km baseline. Because we are interested in the scales $\ell \sim 2000$, we take $D = 1$ km and $A/T = 1000\,{\rm m^2\,K^{-1}}$. The sky fraction $f_{\rm sky}$ corresponds to the one of SKA because we consider *Planck* as CMB observation, which is almost full sky. We assume 200 deg^2 per field of view and four independent survey fields for SKA. Therefore the total sky fraction is $f_{\rm sky} \sim 0.02$.

We plot S/N as a function of $t_{\rm obs}$ in units of hours for 'stars' and 'QSOs' models at $z = 11$ in Fig. 5. In both panels in Fig. 5, S/N of SKA with *Planck* is represented by the solid lines. Obviously, longer observation times make S/N larger. Then, since the cross-correlation amplitude in the 'QSOs' model is higher than in the 'stars' model, S/N in the former model is lager than in the later model. However both S/N are below the detection level. This difficulty of the detection is mainly due to the instrumental noise of the 21-cm observation. Although the primary CMB is one of the significant sources of noise in the detection of the cross-correlation signal between CMB and 21 cm from EoR on large scales (Jelić et al. 2010; Tashiro et al. 2010), the primary CMB suffers Silk damping on the scales we are interested in here and the noise of *Planck* is also kept below the sufficient level.

In order to clarify the impact of the improvement in the sensitivity of 21-cm observation, we calculate S/N in the case of a 5 times better sensitivity than that of SKA and plot the result as the dotted line in Fig. 5. The improvement of the sensitivity of 21-cm observation brings

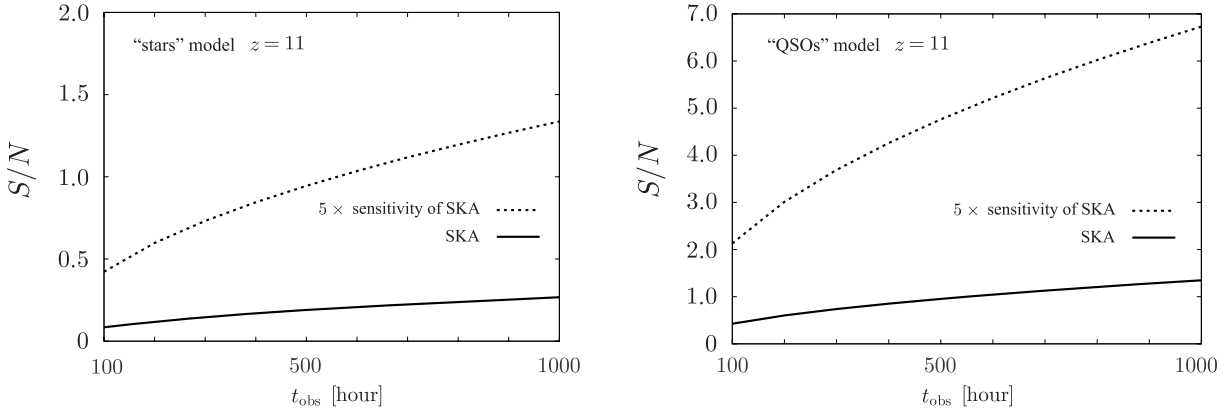

Figure 5. The S/N ratio for the detection of the cross-correlation signal at $z = 11$ as a function of the observation time. The left-hand panel is for the 'stars' model and the right-hand panel is for the 'QSOs' model. In both panels, the solid and dotted lines represent S/N for SKA and for the observation with a 5 times better sensitivity than that of SKA, respectively. We set $f_{\rm sky} \sim 0.02$ in all plots.

large S/N. Especially, the S/N in the 'QSOs' model can reach S/N ~ 5 in 500-h observation. Finally, while we use the same sky fraction $f_{\rm sky} \sim 0.02$ in all calculations, larger sky fractions also make S/N higher.

5 CONCLUSION

We investigated the small-scale cross-correlation between CMB anisotropies and the 21-cm fluctuations during the EoR in harmonic space. The CMB anisotropies at small scales are mainly caused by the kSZ effect which is the second-order fluctuation effect generated by the peculiar velocity and the fluctuations of the visibility function. We therefore calculated the cross-correlation with the second-order fluctuations of 21-cm fluctuations.

The cross-correlation signal between kSZ and 21-cm fluctuations is negative on small scales. This anti-correlation on small scales was found in the numerical simulations of Salvaterra et al. (2005) and Jelić et al. (2010). We found that the position of the negative peak is at the angular scale corresponding to the typical size of an ionized bubble at the redshift probed by 21-cm fluctuation measurements. This angular scale shifts to smaller scales as ionized bubbles evolve. The amplitude also increases with the reionization process until the average ionization fraction reaches $\bar{x}_{\rm i} \sim 0.9$. The amplitude of the cross-correlation strongly depends on the typical bubble size. The cross-correlation in the case of larger bubbles has a higher amplitude than in the case of smaller bubbles, even if in both cases the mean ionization fractions are the same. Moreover, the amplitude of the cross-correlation from large ionized bubbles is comparable to that of the first-order cross-correlation. Those characteristic features of the cross-correlation could be used to distinguish between different reionization histories with future observations.

We also estimated the detectability of the small-scale cross-correlation by the current design sensitivity of SKA. It is rather difficult to detect the cross-correlation signal even in the radical reionization cases. However, if the sensitivity is improved by a factor of 5, the detection or non-detection of the cross-correlation signal will definitely provide information about the EoR.

ACKNOWLEDGMENTS

HT is supported by the Belgian Federal Office for Scientific, Technical and Cultural Affairs through the Interuniversity Attraction Pole P6/11.

REFERENCES

Adshead P. J., Furlanetto S. R., 2008, MNRAS, 384, 291
Aghanim N., Majumdar S., Silk J., 2008, Rep. Progress Phys., 71, 066902
Alvarez M. A., Komatsu E., Doré O., Shapiro P. R., 2006, ApJ, 647, 840
Barkana R., Loeb A., 2004, ApJ, 601, 64
Bharadwaj S., Ali S. S., 2004, MNRAS, 352, 142
Bouwnes R. J. et al., 2010, preprint (arXiv:1006.4360)
Ciardi B., Madau P., 2003, ApJ, 596, 1
Cooray A., 2004, Phys. Rev. D, 70, 063509
Dvorkin C., Hu W., Smith K. M., 2009, Phys. Rev. D, 79, 107302
Fan X. et al., 2006, AJ, 132, 117
Furlanetto S. R., Zaldarriaga M., Hernquist L., 2004a, ApJ, 613, 16
Furlanetto S. R., Zaldarriaga M., Hernquist L., 2004b, ApJ, 613, 1
Furlanetto S. R., Oh S. P., Briggs F. H., 2006, Phys. Rep., 433, 181
Jelić V. et al., 2010, MNRAS, 402, 2279
Knox L., 1995, Phys. Rev. D, 52, 4307
Komatsu E. et al., 2011, ApJS, 192, 18
Lacey C., Cole S., 1993, MNRAS, 262, 627
McQuinn M., Furlanetto S. R., Hernquist L., Zahn O., Zaldarriaga M., 2005, ApJ, 630, 643
Madau P., Meiksin A., Rees M. J., 1997, ApJ, 475, 429
Masi S. et al., 2008, Mem. Soc. Astron. Ital., 79, 887
Miralda Escudé J., 1998, ApJ, 501, 15
Ostriker J. P., Vishniac E. T., 1986, ApJ, 306, L51
Salvaterra R., Ciardi B., Ferrara A., Baccigalupi C., 2005, MNRAS, 360, 1063
Sheth R. K., 1998, MNRAS, 300, 1057
Slosar A., Cooray A., Silk J. I., 2007, MNRAS, 377, 168
Sunyaev R. A., Zel'dovich I. B., 1980, MNRAS, 190, 413
Tashiro H., Aghanim N., Langer M., Douspis M., Zaroubi S., 2008, MNRAS, 389, 469
Tashiro H., Aghanim N., Langer M., Douspis M., Zaroubi S., Jelić V., 2010, MNRAS, 402, 2617
Trac H., Gnedin N. Y., 2009 (ArXiv:0906.4348)
Vishniac E. T., 1987, ApJ, 322, 597
Zahn O., Zaldarriaga M., Hernquist L., McQuinn M., 2005, ApJ, 630, 657
Zaldarriaga M. and Furlanetto S. R. and Hernquist L., 2004, ApJ, 608, 622
Zel'dovich Y. B., Sunyaev R. A., 1969, Astrophys. Space Sci., 4, 301

This paper has been typeset from a TEX/LATEX file prepared by the author.